日本建築学会技術報告集　第19巻　第41号，179-184，2013年2月
AIJ J. Technol. Des. Vol. 19, No.41, 179-184, Feb., 2013

THE EFFECT OF HUMIDITY ON THE STABILITY OF PRESSURE - VELOCITY SENSORS
－ A measurement method of absorption characteristics of building materials by using ensemble averaging －

音圧－粒子速度センサの安定性への湿度の影響
－アンサンブル平均を利用した建築材料の吸音特性測定法－

Asniawaty KUSNO ―― ＊1　**Toru OTSURU** ―― ＊2
Reiji TOMIKU ―― ＊3　**Noriko OKAMOTO** ―― ＊4
Nazli BIN CHE DIN ―― ＊5

アスニアワティ クスノ―― ＊1　大鶴　徹―― ＊2
富来礼次 ―― ＊3　岡本則子―― ＊4
ナズリ ビン チェ ディン―― ＊5

Keywords:
Sound absorption measurement, Pressure-velocity sensor, Relative humidity

キーワード：
吸音測定，音圧–粒子速度センサ，相対湿度

To examine humidity influence on stability of pu-sensors, we applied calibration and the ensemble averaged surface normal impedance method (EA-Method) under controlled relative humidity (φ=35-60%) in a reverberation room. Experiments revealed that calibration results (i.e. correction values) changed as humidity levels varied. A comparison of standard deviations on absorption coefficients generated increasing value as the humidity difference between calibration and measurement increased ($\Delta\varphi$=0-25%). Repeatability was demonstrated by using two identical pu-sensors in four set measurements. Furthermore, a partial correlation test demonstrated the dominance of humidity over other environmental factors influencing sensor sensitivity.

1. Introduction

Various methods have been proposed for measuring sound absorption characteristics of materials especially for buidings[1–10]. Some recent studies have used pressure-velocity probes (pu-sensors)[4-10]. Using these sensors, the authors proposed another method (EA-method) to measure the surface normal impedance of a material by application of an ensemble-averaging technique[6,8-10].

In one application of pu-sensors, Jacobsen *et al.* conducted sound absorption and intensity measurements, and then reported some uncertainties related to sensor calibration methods[11] recommended in the manufacturer's instruction manual[12]. Additionally, Basten and de Bree presented a procedure to conduct calibration of the pu-sensor in a wide range[13].

In previous papers[6,8-10], the authors conducted a series of EA-method measurements by applying the manufacturer's recommendations to the calibration method. To ensure accuracy, the stability of the transfer function on sound pressure and particle velocity resulting from the calibration process were monitored. We encountered another point of uncertainty attributable to the instability of the monitored transfer function, and thus we inferred that sensor instability might be influenced by humidity surrounding the pu-sensor.

Svetovoy *et al*[14] and Honschoten *et al*[15] discussed in their paper about microflown (μ-flown) sensor stability and mechanism on temperature changes using a geometric analytical model. The μ-flown is the particle velocity sensor that is used in a pu-sensor. The design principle of the μ-flown sensor is simply the heat difference sensed by two parallel wires. The heat difference depends on thermal conductivity and it might be affected by humidity. However, Svetovoy *et al* and Honschoten *et al* assumed the thermal conductivity to be constant and did not examine the influence of humidity on the model.

The pu-sensor manufacturer detected the influence of ambient temperature, atmospheric pressure, and humidity to pu-sensor sensitivity. The figures presented by de Bree[12] show the influence of atmospheric pressure affected within high-frequency ranges above 1500 Hz with less than 0.05 dB. The ambient temperature affected the frequency range above 750 Hz by less than 1 dB. In contrast, the humidity influence affected all frequency ranges by 3.5 dB[12].

Therefore, we will examine the relative humidity influence on pu-sensor stability through measurements consisting of calibrations and EA-method measurements. Furthermore, the focus of the study is on explaining the importance of considering the humidity factors related to the pu-sensor stability in order to produce more reliable results of absorption coefficients. The result will be useful not only

*1 Graduate Student, Graduate School of Eng., Oita Univ., Dept. of Architecture, Faculty of Eng. Hasanuddin Univ., Indonesia., M. Eng.
*2 Prof., Dept. of Architecture and Mech., Oita Univ., Dr. Eng.
*3 Assoc. Prof., Dept. of Architecture and Mech., Oita Univ., Ph. D.
*4 Assistant Prof., Ariake National College of Technology., Ph. D.
*5 Dept. of Architecture, Faculty of Built Env., Univ. of Malaya, Malaysia., Ph. D.

*1 大分大学大学院工学研究科／ハサヌディン大学インドネシア　工修（〒870-1192　大分市旦野原700番地）
*2 大分大学工学部　教授・工博
*3 大分大学工学部　准教授・博士（工学）
*4 有明工業高等専門学校建築学科　助教・博士（工学）
*5 マラヤ大学マレーシア　博士（工学）

for EA-method measurement but also for various methods of architectural acoustics measurement.

2. Methodology

2.1. Calibration Method in Impedance Tube

In this study, we use an impedance tube to calibrate the pu-sensors. As presented in Fig. 1, the tube has length L; its end is terminated by a hard wall.

Hereinafter, i is an imaginary number $\sqrt{-1}$, and ω is the angular frequency. Then, both measured sound pressure $p_{\mathrm{m}}(X)$ and measured particle velocity $u_{\mathrm{m}}(X)$ are measured by using the pu-sensor located at point X.

To calculate the true transfer function $H_{\mathrm{up\_t}}(\omega)$ between the particle velocity and sound pressure, a correction value, C_{H}, is defined as follows:

$$H_{\mathrm{up\_t}}(\omega) = H_{\mathrm{up\_m}}(\omega) \cdot C_{\mathrm{H}} \ , \tag{1}$$

$$C_{\mathrm{H}} = \frac{\rho c \cos\left(k\,[L - X]\right)}{i \sin\left(k\,[L - X]\right)} \cdot \frac{u_{\mathrm{m}}(X)}{p_{\mathrm{m}}(X)} \ , \tag{2}$$

Therein, $H_{\mathrm{up\_m}}(\omega)$ denotes a measured transfer function using the pu sensor, k signifies the wave number, ρ represents air density, and c stands for the speed of sound. Theoretically, C_{H} is independent of X.

2.2. Ensemble Averaged Impedance (EA-method) and Corresponding Absorption Coefficient

In previous papers[6,8-10], the authors introduced impedance as

$$\langle Z_{\mathrm{n}} \rangle = \frac{\langle p \rangle}{\langle u_{\mathrm{n}} \rangle}, \tag{3}$$

where p and u_{n} denote the sound pressure and particle velocity with respect to the normal direction at the material surface, and where $< \bullet >$ denotes ensemble averaging at random incidence. Tentatively, the resulting impedance, $<Z_{\mathrm{n}}>$, was designated as "Ensemble Averaged" impedance. The authors defined the "corresponding absorption coefficient" $<\alpha>$, to check and to evaluate the impedance as follows:

$$\langle \alpha \rangle = 1 - \left| \frac{\langle Z_{\mathrm{n}} \rangle - \rho c}{\langle Z_{\mathrm{n}} \rangle + \rho c} \right|^2 . \tag{4}$$

In practical measurements, the averaging of calibration performed using a fast Fourier transform (FFT) was conducted as

$$\langle Z_{\mathrm{n}} \rangle = \frac{1}{N} \sum^{N} H_{\mathrm{up_t}}(\omega) \ , \tag{5}$$

where N is the averaging number used in FFT. Here, the incident condition for obtaining $<Z_{\mathrm{n}}>$ is random and the average value of the impedances over incident angles is derived. For a system that is ergodic and assuming sufficient averaging, Eqs. (3) and (5) become identical. Then, we can measure the averaged surface normal impedance at random incidence.

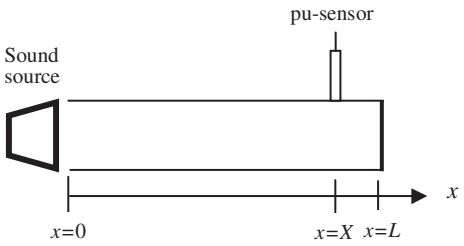

Fig. 1 Schematic diagram of pu-sensor calibration in an impedance tube.

3. Measurements

3.1. Setting of Calibration

To conduct practical calibrations, as shown in Fig. 1, the pu-sensor was calibrated by application of a square impedance tube with 70 cm long, L, and 10 cm × 10 cm inner dimensions. The pu-sensor positioned at point X = 68 cm. Pink noise was emitted from a loudspeaker at the opening edge of a tube (x=0). The resolution of two-channel FFT unit (SA-78; Rion Co. Ltd.) was set to 1.25 Hz by length of Hanning window 0.8 s. Linier averaging of N=150 in the frequency domain was performed in 90 seconds because of the time overlap.

3.2. Setting of EA-method Measurement

Figure 2 depicts a schematic diagram of EA-method measurement setup with pu-sensor utilization[6,8–10]. The pu-sensor is positioned at the center of 0.9 m × 0.9 m sample material. Distance, d, is 1 cm above the material surface. Glass wool (GW50) with 32 kg/m^3 density and 50 mm in thickness is used as the measured material. The same settings of two-channel FFT in Section 3.1 were applied.

As described in our previous papers[6,8-10], to produce the incidence condition close to random incidence, six loudspeakers (FE-103; Fostex Co.) mounted in small boxes that radiate incoherent pink noise were placed in a reverberation room. The pink noise was filtered to focus on the frequencies of 100–1200 Hz. A sub-woofer (SX-DW77; Victor, Ltd.) was also installed to increase the low-frequency energy, roughly below 200 Hz.

3.3. Measurement Conditions

Measurements and calibrations were conducted in a reverberation room of 168 m^3 with non-parallel reinforced concrete walls, located in the basement of Oita University Information Center. In this section, each calibration and the EA-method measurement of the pu-sensor are referred to as a *pair*. Each pair is taken at the same humidity level (difference of humidity, $\Delta\varphi$ = 0%). Because time durations of both measurements (the calibration and the EA-method measurements) were 90 seconds each, we predicted that the environmental conditions might not change significantly. To

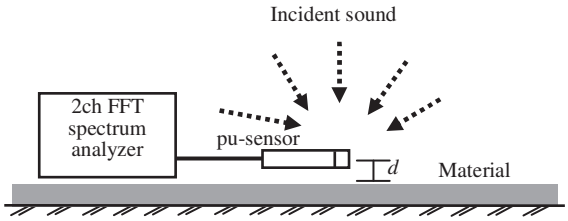

Fig. 2 Schematic diagram of the EA-method measurement setup with a pu-sensor.

maintain humidity condition at $\Delta\varphi = 0\%$, the measurement using the EA-method was conducted immediately after the pu-sensor calibrated.

The level of relative humidity is conditioned to increase gradually by 5% intervals, starting from humidity 35–60%, and resulting in six pairs of calibration and EA-method measurement at the same level of humidity. Complete pairs of calibration and EA-measurement on six levels of humidity comprise one *set,* and due to the amount of time needed to control and maintain room humidity, one set measurement usually took 1–2 days. Each set of measurements was taken by using two identical pu sensors in turn. These sensors were labeled as pu-1 and pu-2 (PT0905-32 and PT0404-05; Microflown Technologies). To demonstrate repeatability, four sets of measurements were conducted over of a period of 390 days from November 2010 to December 2011. Set 1 was conducted in December 2010; set 2 in October 2011; set 3 and 4 in December 2011.

The relative humidity inside the room was controlled using a humidifier (KA-N35; Toshiba Corp.) and dehumidifier (MJ-180EX; Mitsubishi Electric Corp.), respectively, to increase and decrease humidity. To obtain uniform relative humidity inside the room, a conditioning fan (YKS-451; Yamazen) was applied before each sensor calibration at each humidity level.

In addition to humidity, ambient temperature and atmospheric pressure were also recorded during the measurement. The ambient temperature and relative humidity were measured by means of a temperature and humidity meter (DT-321S; CEM Corp.) with the precision of ±0.5°C and ±2% respectively. The atmospheric pressure was also measured using a barometer attached to a pistonphone (NC-72; Rion Co. Ltd.). During the period of 90 seconds while the measurements were being taken, the temperature and humidity meter as well as the barometer were positioned at a distance of 1 m from the pu-sensor. The uniformity of humidity was confirmed within a range ± 1% during the measurements at each humidity level by visual observation. The temperature ranges while measurements were being taken on each set were as follows: Set 1 is from 19.6-20.7°C; set 2 is 22.4-24.3 °C; set 3 is 19.6-20.4 °C; and set 4 is 19.6-20.3 °C. The changes of atmospheric pressure on each set measurement are slight where the maximum difference is 0.7 kPa.

4. Results and Discussions

4.1. Relation between humidity and correction value on sensors calibration

In all measurements, similar procedures for both pu-1 and pu-2 sensors were applied where the results of calculated C_H demonstrated comparable trends. Therefore, in view of this, only one of the sets was used (set 4) to illustrate the similar phenomena of the other measurement sets.

The influence of relative humidity on the results of pu-sensor calibration in six relative humidity levels, φ, of 35–60% by 5% humidity intervals was examined. To give the tendency clearer for visual observations, the real parts and imaginary parts are illustrated hereafter instead of amplitude and phase.

Figure 3(a) portrays frequency characteristics of the correction value, C_H, of pu-1 at six relative humidity levels of 35%–60%. In the figure, the six relative humidity levels are shown as parameters. The frequency characteristics of real parts for the six correction values show a sequential order from $\varphi = 35\%$ to $\varphi = 55\%$ at frequencies of 100 Hz–1200 Hz. At $\varphi = 60\%$, C_H is obtained between $\varphi = 45\%$ and $\varphi = 50\%$. The imaginary part of C_H at $\varphi = 55\%$ and $\varphi = 60\%$ above frequency 650 Hz tend to agree each other. Similarly, C_H of $\varphi = 35\%$, $\varphi = 40\%$, $\varphi = 45\%$, and $\varphi = 60\%$

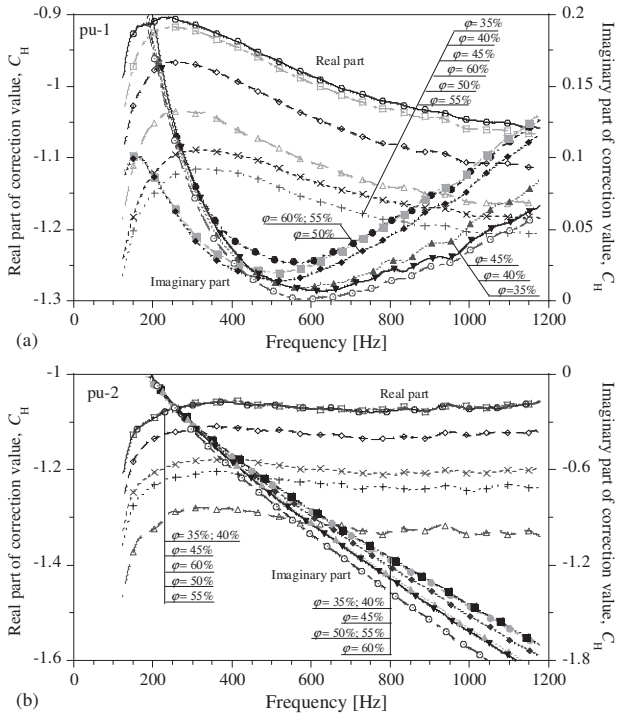

Fig. 3 Correction value, C_H, at different relative humidity from $\varphi = 35\%$ to $\varphi = 60\%$: (a) pu-1 and (b) pu-2**.**

from frequencies of 200–300 Hz agree as well as φ = 50% and φ = 55%. The imaginary part of C_H then spreads and forms a sequential order from φ = 35% to φ = 60%.

Figure 3(b) shows frequency characteristics of the correction value, C_H, of pu-2 at different relative humidity from φ = 35% to φ = 60%. The real part of C_H at 35% and 40% agree each other well across the frequency region. Nevertheless, a sequential order of C_H from φ = 35% to φ = 60% occurred here. All C_H of the imaginary part agree within the frequency range of 200–300 Hz, then tend to spread and form a sequential order of φ = 40% to φ = 60% from 300 Hz to the upper frequencies. However, especially for φ = 35% and φ = 40% as well as φ = 50% and φ = 55% agree in the frequency range of 200–1200 Hz.

In Figs. 3(a) and 3(b), we can observe gradual changes of C_H according to the humidity both for pu-1 and pu-2. It might not be clear that the change is exactly in the sequential order of humidity, but the change represents a kind of humidity effect onto the result of pu-sensor in a simple application. In the following sections, the influence of C_H on measurement results using EA-method will be discussed.

4.2. Relation between humidity and absorption characteristics measured in the same humidity ($\Delta\varphi$ = 0%)

This section provides the comparison of normalized impedances, ($<Z_n>/\rho c$), and absorption coefficients, $<\alpha>$, measured by using the EA-method for a combination of the same relative humidity, both in calibrations and measurements (i.e. $\Delta\varphi$ = 0%). $\Delta\varphi$ is the group of certain relative humidity difference.

The impedance value $<Z_n>$ was calculated from the transfer function H_{up_t} obtained using H_{up_m}, which were measured at certain relative humidity then multiplied by the correction value C_H obtained at calibration on certain relative humidity.

A comparison of $<Z_n>$ or $<\alpha>$ on the pair combinations were made as follows: first, the moving averages of $<Z_n>$ and $<\alpha>$ are calculated with 50 Hz steps. The author designates such values as Z'_{cm} and α'_{cm}. Secondly, the impedance and absorption coefficient over combinations are calculated in arithmetic means, then denote as $\overline{Z}'_{\Delta\varphi}$ and $\overline{\alpha}'_{\Delta\varphi}$, respectively.

Among six pairs combinations of calibration and measurement with the same relative humidity (Table 1: $\Delta\varphi$ = 0%), only the value of the maximum, the minimum and the arithmetic means of impedances Z'_{cm} and absorption coefficients α'_{cm} are illustrated in Fig. 4.

Figure 4(a) shows frequency characteristics of impedances obtained by pu-1 and pu-2. In the figure, some discrepancies are observed among the value of the maximum, the minimum and the arithmetic mean within six pairs of impedance Z'_{cm} especially in the low-frequency range below about 250 Hz. Even so, overall agreement within the combinations is good in both real and imaginary parts of the impedances.

Table 1 Complete set of measurement and examination consist of six groups and each group consists of pairs

[**Group**] Difference of Relative humidity, $\Delta\varphi$	[**Combination of Pair**] Calibration (c) and EA-Measurement (m)
0%	c35m35, c40m40, c45m45, c50m50, c55m55, c60m60
5%	c35m40, c40m45, c45m50, c50m55, c55m60, c40m35, c45m40, c50m45, c55m50, c60m55
10%	c35m45, c40m50, c45m55, c50m60, c45m35, c50m40, c55m45, c60m50
15%	c35m50, c40m55, c45m60, c50m35, c55m40, c60m45
20%	c35m55, c40m60, c55m35, c60m40
25%	c35m60, c60m35

Next, Fig. 4(b) shows frequency characteristics of the corresponding absorption coefficients obtained by pu-1 and pu-2. Throughout the frequency range except at 125 Hz, the small width between the maximum and minimum values at a frequency show that the absorption coefficients at a frequency agree well each other within the combinations of $\Delta\varphi$ = 0. Similar agreements can be observed both for pu-1 and pu-2.

The general agreements among impedances and

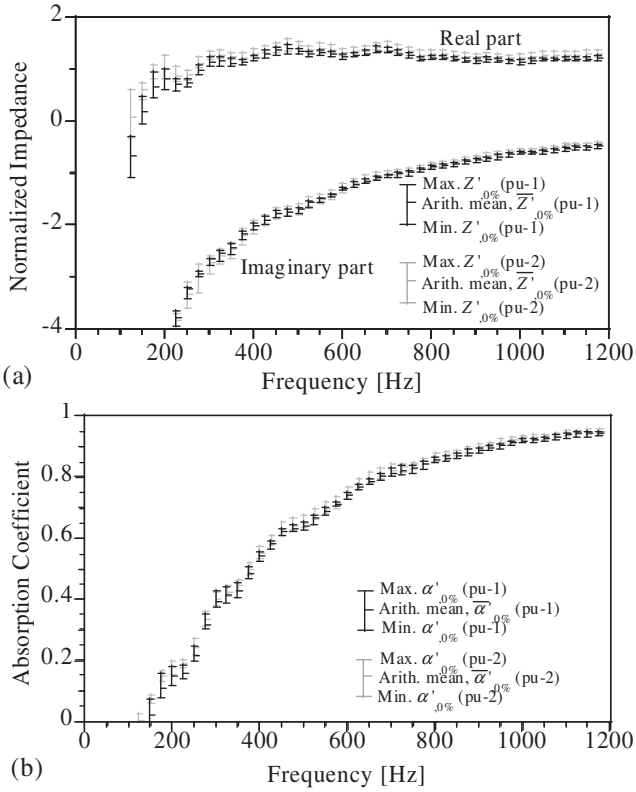

Fig. 4 Maximum, minimum, and arithmetic mean value of absorption characteristics of GW50 within the group of $\Delta\varphi$ = 0%; (pu-1 and pu-2)

among absorption coefficients measured by using pu-1 and pu-2 are resulted mainly from the same measurement conditions, where each calibration and EA-method measurement of the pu-sensor was taken at the same humidity level (difference of humidity, $\Delta\varphi = 0\%$). Under this condition, the calibration results C_H are considered accurate enough to produce consistent measurement results of impedance and its corresponding absorption coefficients. A similar tendency of the above results also occurred in the other measurement sets. An examination of other $\Delta\varphi$ is explained in the next section.

4.3. Examination on Six Groups of Humidity Difference ($\Delta\varphi > 0\%$)

An extensive examination was conducted to clarify the influence of humidity on pu-sensor sensitivity. The examinations were applied through calculation on combination of pairs from humidity difference, $\Delta\varphi$, 5%–25%.

The pairs discussed in this section were obtained from all possible combinations on each humidity difference, $\Delta\varphi$, using previous C_H and impedance values which were measured under humidity conditions from 35% to 60% given in Sec. 4.2. As shown in Table 1, there are 36 combinations of pairs in total, including the pairs measured at the same humidity ($\Delta\varphi = 0\%$),

4.3.1. Standard Deviation of Absorption Coefficients

To examine the absorption coefficients measured of six $\Delta\varphi$, comparisons of standard deviation, SD, were made among the absorption coefficients. The standard deviation is calculated as

$$\mathrm{SD}_{\Delta\varphi}(f) = \sqrt{\frac{1}{N_{\Delta\varphi}} \sum_{\mathrm{cm}}^{N_{\Delta\varphi}} \left(\alpha'_{\mathrm{cm},\,\Delta\varphi}(f) - \bar{\alpha}'_{\Delta\varphi}(f)\right)^2}\,, \qquad (6)$$

where $N_{\Delta\varphi}$ denotes the number of pair of combinations within the group of $\Delta\varphi$.

Figure 5(a) and 5(b) illustrate the frequency characteristics of $\mathrm{SD}_{\Delta\varphi}(f)$ obtained by pu-1 and pu-2 respectively. In Fig. 5(a), $\mathrm{SD}_{\Delta\varphi}(f)$s are apparently deviated sequentially from the lowest $\Delta\varphi = 0\%$ to $\Delta\varphi = 25\%$ in the frequency region above 275 Hz. As an exception, for frequency below 275 Hz, the $\mathrm{SD}_{\Delta\varphi}(f)$ is distributed randomly. Meanwhile, for pu-2 in Fig. 5(b), sequence tendencies also occurred, except $\mathrm{SD}_{\Delta\varphi}(f)$s for $\Delta\varphi = 25\%$ and 20% which was almost identical.

Here, the sequential increasing of $\mathrm{SD}_{\Delta\varphi}(f)$s from $\Delta\varphi = 0\%$-25%, show evidence that the difference of humidity between the measurement of calibration and the EA-measurement lead to dispersion of the resulting

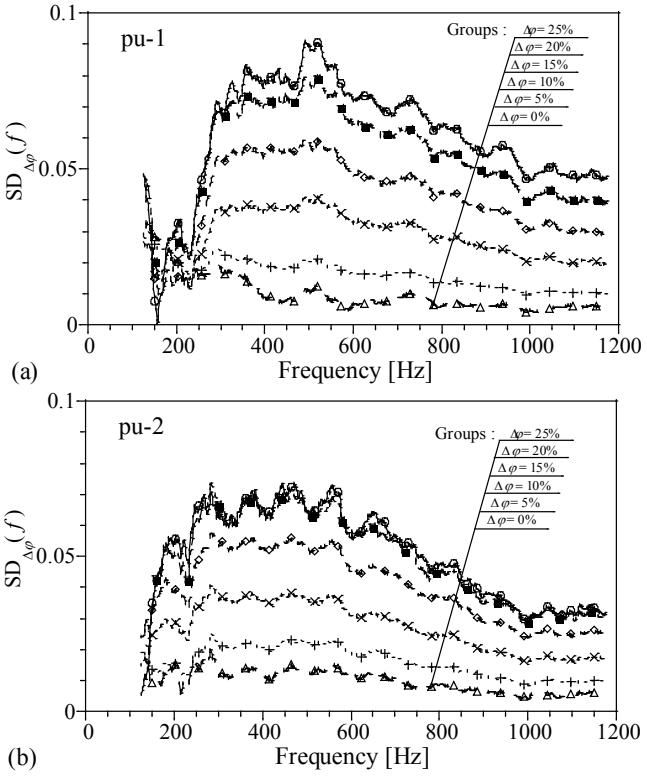

Fig. 5 Comparisons of standard deviations ($\Delta\varphi = 0$, 5, 10, 15, 20 and 25%): (a) pu-1 and (b) pu-2.

absorption coefficients. In this case, the $\mathrm{SD}_{\Delta\varphi}(f)$s of $\Delta\varphi = 0\%$ has the smallest deviation compared to other $\Delta\varphi$, meaning that calibration and EA-method measurement under humidity $\Delta\varphi = 0\%$ yield the most stable result.

Further analysis of $\mathrm{SD}_{\Delta\varphi}(f)$ is presented in Fig. 6 to explain the results of all sets. In the figure, $\mathrm{SD}_{\Delta\varphi}(f)$ is averaged over frequencies of 125–1175 Hz and denoted as $\overline{\mathrm{SD}}_{\Delta\varphi}$. The figure shows eight $\overline{\mathrm{SD}}_{\Delta\varphi}$ values with respect to the difference of relative humidity, $\Delta\varphi$, from 0%-25%. The eight $\overline{\mathrm{SD}}_{\Delta\varphi}$ values consist of four sets of measurement, where each set of measurement obtained by using pu-1 and pu-2.

Regardless of the sensors, $\overline{\mathrm{SD}}_{\Delta\varphi}$ increases with increasing $\Delta\varphi$ occurred from 0%-25%, and the tendency

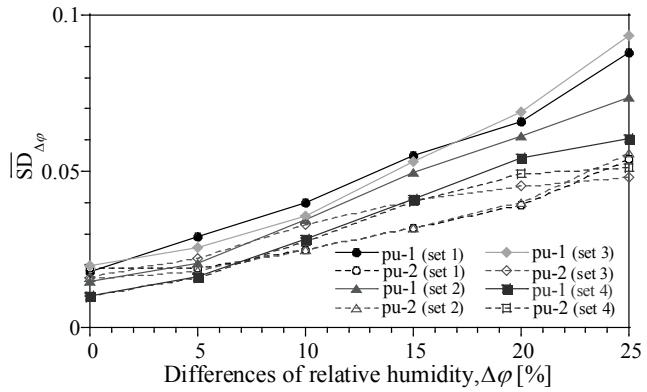

Fig. 6 Standard deviation, $\overline{\mathrm{SD}}_{\Delta\varphi}$ with respect to the difference of relative humidity, $\Delta\varphi$, from 0%-25% obtained by pu-1 and pu-2.

repeatedly occurred within a long period of time. As a reference, if the $\Delta\varphi$ is less than 10%, $\overline{SD}_{\Delta\varphi}$ less than 0.05 can be expected in frequency region above 250 Hz. In this study, there were three limitations of the measurement conditions: Firstly, the humidity ranged from 35-60%, secondly, the maximum difference of temperature was 1.8°C and thirdly, the maximum difference of atmospheric pressure was 0.7 kPa.

4.4. Statistical Analysis of Environmental Factors Influences

The ambient temperature and atmospheric pressure are two other environmental factors that possibly influence sensor sensitivity during the process of application. Therefore, as additional information, the influence of respective environmental factors on the sensor sensitivity was calculated by means of the partial correlation test.

The partial correlation results between the $\overline{SD}_{\Delta\varphi}$ of the absorption coefficient and the SD of the temperature (Δt), atmospheric pressure (Δp), and humidity ($\Delta\varphi$), are shown in Table 2.

Table 2 Partial correlation

	$\Delta\varphi$	Δp	Δt
pu-1	0.955	0.521	-0.069
pu-2	0.959	0.160	-0.461

Both calculated results of pu-1 and pu-2 showed coefficient number > 0.95, which explains the significant correlation of $\Delta\varphi$ on the sensor stability. Up to this stage, $\Delta\varphi$ has the most significant influence on $\overline{SD}_{\Delta\varphi}$ among other environmental factors. It should be noted that the investigation of these factors are limited within the range mentioned in Sec. 4.3.1.

5. Conclusions

The authors examined the stability of pu-sensor measurement through the changes of relative humidity, ranged from 35%–60% in a reverberation room. Here, the change in humidity influences the C_H value. Comparisons of standard deviations result on absorption coefficients for six groups of different relative humidity from 0%-25% indicate that humidity exerts a significant influence on the sensors, where the deviation values increases as the humidity difference increases and the tendency occurred within a long period. Hence, measurements performed under the same humidity condition will produce more stable absorption coefficients. For practical use, limitation of deviation might be required for specific measurement and $\Delta\varphi$ is necessary to be considered. Partial correlation test on environmental factors that may affect the sensors stability confirmed that there is considerable influence of humidity on the deviation values of absorption coefficients. Finally, the present study concludes that humidity plays a non-negligible role in the stability of pu-sensors at some applications.

Acknowledgements

This study was conducted as a Research Fund at the Discretion of the President, Oita University. The author was supported by the Ministry of Higher Education, Indonesia, 2008–2011. The authors also would like to thank to Dr. T. Okuzono, Ms. C. Ueki, Ms. R. Matsumoto, Mr. H. Nakano, Ms. M. Ohnishi, Mr. K. Kamil and Mr. T. Harran for their contributions.

References

1) J. F. Allard and Y. Champoux.: In Situ Two-Microphone Technique for The Measurement of The Acoustic Surface Impedance of Materials, Noise Control Eng. J., Vol. 32, pp. 15–23 (1989).
2) M. Garai.: Measurement of The Sound-Absorption Coefficient In Situ: The Reflection Method Using Periodic Pseudo-Random Sequences of Maximum Length, Appl. Acoust., Vol. 39, pp. 119–139 (1993).
3) Y. Takahashi *et. al.* .: In Situ Measurements of Surface Impedance and Absorption Coefficients of Porous Materials Using Two Microphones and Ambient Noise, Appl. Acoust., Vol. 66, pp. 845–865 (2005).
4) K. Hirosawa *et. al.:* Comparison of Three Measurement Techniques for The Normal Absorption Coefficients of Sound Absorbing Materials In The Free Field, J. Acoust. Soc. Am., Vol. 126, pp. 3020–3027 (2009).
5) L. Yang and F. Jacobsen.: Measurement of Absorption with a P-U Sound Intensity Probe In an Impedance Tube (L)," J. Acoust. Soc. Am., Vol. 118, pp. 1–4 (2005).
6) T. Otsuru *et. al.:* Ensemble Averaged Surface Normal Impedance of Material Using an *In-Situ* Technique: Preliminary Study Using Boundary Element Method, J. Acoust. Soc. Am., Vol. 125, pp. 3784–3791 (2009).
7) E. Brandão *et. al.:* A Comparison. of Three Methods to Calculate The Surface Impedance & Absorption Coefficients From Measurements Under Free Field or In Situ Conditions, Acta Acustica United with Acustica., Vol. 97, pp. 1025–1033 (2011).
8) T. Otsuru *et. al.:* Ensemble Averaged Surface Normal Impedance Measurement Method In a Reverberation Room, Acoust. Sci. & Tech., Vol. 32, pp. 69–71 (2011).
9) N. B. C. Din *et. al.*: Measurement Method with a Pressure-Velocity Sensor for Measuring Surface Normal Impedance of Materials Using Ensemble Averaging: Comparison With Other Methods and Its Geometrical Configuration., Acoust. Sci. & Tech., Vol. 33, pp. 86–95 (2012).
10) N. B. C. Din *et. al*.: An *In-Situ* Technique for Extensive Field Measurements of Absorption Characteristics of Materials by Using Ensemble Averaging, Proc. 20th Int. Congr. Acoust., pp. 820-824 (2010), on CD ROM.
11) F. Jacobsen and V. Jaud.: A Note on The Calibration of Pressure–Velocity Sound Intensity Probes, J. Acoust. Soc. Am., Vol. 120, 830–837 (2006).
12) H-E. de Bree.: The Microflown E-book H-E de Bree, Chap. 4A.7, 12-14, available online at <http://www.microflown.com/ files/media/ library/books/microflown_ebook/ebook_4a_standar_calibration_techniques.pdf>(last viewed 4/17/2011).
13) T. Basten and H-E. de Bree.: Full Bandwidth Calibration Procedure for Acoustic Probes Containing a Pressure and Particle Velocity Sensor, J. Acoust. Soc. Am., Vol. 127, pp. 274–270 (2010).
14) V. B. Svetovoy and I. A. Winter.: Model of The μ-Flown Microphone, Sensors and Actuators, Vol. 86, pp. 171–181 (2000).
15) J. W. van Honschoten *et. al.:* Optimization of a Two-Wire Thermal Sensor for Flow and Sound Measurements, Proc. The 14th IEEE Int. Conf., pp. 523-526 (2001).

[2012 年 6 月 20 日原稿受理　2012 年 8 月 7 日採用決定]